Structural, Photophysical, and Nonlinear Absorption Properties of *trans*-Di-arylalkynyl Platinum(II) Complexes with Phenyl and Thiophenyl Groups

Per Lind,[†] Dan Boström,[‡] Marcus Carlsson,[†] Anders Eriksson,[||] Eirik Glimsdal,[§] Mikael Lindgren,[§] and Bertil Eliasson*[,†]

Department of Chemistry, Organic Chemistry, Umeå University, SE-901 87 Umeå, Sweden, Energy Technology and Thermal Process Chemistry, Umeå University, SE-901 87 Umeå, Sweden, Department of Physics, Norwegian University of Science and Technology, NO-7491 Trondheim, Norway, and Division of Sensor Technology, Swedish Defence Research Agency (FOI), SE-581 11 Linköping, Sweden

Received: October 6, 2006; In Final Form: November 22, 2006

Optical power limiting and luminescence properties of two Pt(II) complexes with thiophenyl and phenyl groups in the ligands, *trans*-Pt(P(*n*-Bu)$_3$)$_2$(C≡C−Ar)$_2$, where Ar = −C_4H_2S−C≡C-*p*-C_6H_4-*n*-C_5H_{11} (**1**) and −*p*-C_6H_4−C≡C−C_4H_3S (**2**), have been investigated. The fluorescence lifetimes were found to be on the sub-nanosecond time scale, and the quantum yields were low, in accord with fast intersystem crossing from the excited singlet to triplet manifold. The phosphorescence lifetimes of **1** and **2** were shorter than that of a Pt(II) complex having two phenyl groups in the ligands. In order to elucidate the C−Pt bonding nature in the ground state, the ^{13}C NMR chemical shift of the carbon directly bonded to Pt, the coupling constants $^1J_{PtC}$, $^2J_{PtC}$, and $^1J_{PtP}$, and IR $\nu_{C\equiv C}$ wavenumbers were obtained for **1**, **2**, and three other *trans*-diarylalkynyl Pt(II) complexes. X-ray diffraction data of **1** and **2** and density functional theory calculated geometries of models of **1**, **2**, and *trans*-Pt(P(*n*-Bu)$_3$)$_2$(C≡C-*p*-C_6H_4−C≡C−C_6H_5)$_2$ (**3**) show that **1** preferably exists in a different conformation from that of **2** and **3**. The variations in photophysical, NMR, and IR data can be rationalized by differences in geometry and π-backbonding from Pt to the alkynyl ligand.

Introduction

It is likely that the developing photonics technology will take advantage of optical nonlinearity in organic and organometallic materials for manipulation of optical signals for various signal processing tasks.[1−3] A class of compounds that has attracted attention for optical nonlinearity is transition metal acetylides, where the rigidity and linear geometry of the alkynyl group has made it an attractive unit in the design of interesting complexes.[4,5] These organometallic complexes can show extraordinary photophysical properties due to the electronic interaction between the transition metal and the organic molecular framework.[6,7] Among the compounds that show large cubic hyperpolarizability, Ru, Ni, and Pt dialkynyl complexes are fairly common.[5] For applications where colorless materials are required, Pt compounds can be of interest since they generally have less absorbance than Ru and Ni compounds in the visible region.[5,8]

Over the last several years, square-planar platinum(II) acetylides (Figure 1) is one group of the transition-metal complexes that has been investigated for two-photon absorption (TPA), excited-state absorption (ESA), and optical power limiting (OPL) of high-intensity light.[9−19]

For OPL applications, a high transmittance of normal-intensity light in the visible region may be desirable. Optical nonlinearity of organic molecules with extended π-electron systems generally increases with conjugation length. However, since this is normally accompanied by decreased transmittance in the visible region, it is crucial to find compounds that display a good balance between the degree of π-electron delocalization and transmittance at these wavelengths. Such conjugated compounds may be comprised of aryl rings separated by other conjugated groups. Because of the comparatively weak absorption of diarylacetylenes in the visible region,[20] the ethynyl group appears to be a suitable bridging unit between aryl groups.

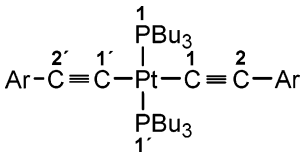

Figure 1. General structure of *trans*-Pt(II) acetylides, with numbering of alkyne carbons as referred to in the text.

In this study, we focus on the molecular structure, optical limiting ability, and luminescence of two new thiophenyl-containing Pt(II) acetylide complexes, **1** and **2** (Figure 2).

Properties of **1** and **2** are compared with those of the structurally related compounds **3** and **4** (Figure 2), both of which have been studied for nonlinear absorption.[9−19] The studies have shown that **3** exhibits optical limiting that is effective for pulse lengths ranging from picoseconds to hundreds of nanoseconds.

Good optical power limiting performance can result from efficient resonant or nonresonant TPA and from ESA when the absorbance is greater than that of the ground state. ESA may involve absorption by a triplet state, which is reached by intersystem crossing (ISC) from an initially populated singlet state. The presence of a heavy metal atom (such as Pt) interacting with a conjugated carbon system in the electronically excited-state can favor ISC by spin−orbit coupling (SOC).[21]

* To whom correspondence should be addressed. E-mail: Bertil.Eliasson@chem.umu.se.
[†] Energy Technology and Thermal Process Chemistry, Umeå University.
[‡] Department of Chemistry, Inorganic Chemistry, Umeå University.
[§] Norwegian University of Science and Technology.
[||] Swedish Defense Research Agency.

10.1021/jp066569p CCC: $37.00
Published on Web 02/10/2007

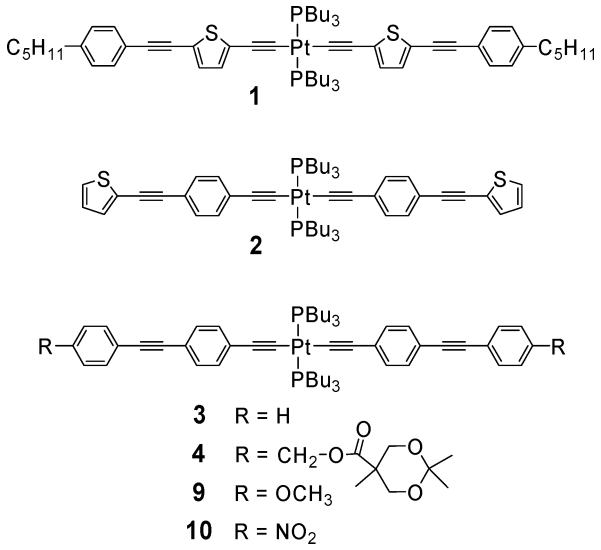

Figure 2. Structures of platinum acetylides **1**−**4**, **9**, and **10**.

In the case of compound **3**, three different wavelength regions of linear and nonlinear absorption of were identified.[11] In the blue region (<500 nm) intersystem crossing followed single-photon absorption from the ground state (S_0) to the first excited state (S_1). In the green region (500−540 nm), a weak absorption due to a direct single photon transition from S_0 to T_1 excited state was found. At longer wavelengths (∼540−700 nm), the excitation pathway was identified as two-photon absorption from S_0 to S_1, followed by ISC to the triplet state.[11]

We have introduced a thiophene ring (thienyl) into this type of structure in an attempt to enhance the optical limiting ability over that displayed by **3**. It has been demonstrated that compounds with conjugated π-systems that incorporate thiophene rings can exhibit large two-photon absorptions at, for instance, 602[22] and 810[23] nm. In addition, studies of thiophene and oligothiophenes show that these structures have fast triplet level formation originating from a TPA-populated singlet excited state.[24−27] This suggests that the presence of the S atom may enhance the TPA, and/or increase the rate of ISC by additional SOC,[28] in Pt acetylides.

The structural data presented here for **1** and **2** include NMR and crystallographic data. The latter are compared with results from quantum chemistry calculations at the density functional theory (DFT) level of theory for compounds **1′**−**3′** having methyl groups in lieu of the butyl and pentyl groups in **1**−**3**. In addition, absorption and emission spectra, excitation energies from time-dependent DFT calculations, time-resolved luminescence data, and results from optical limiting measurements at three wavelengths (532, 550, and 610 nm) are presented.

Experimental Section

Solvents and Reagents. Solvents for synthesis were dried and distilled prior to use. Tetrahydrofuran (THF) from Sigma-Aldrich Co. for spectrometry was of spectrophotometric grade, ≥99.5%. Reagents were obtained from Sigma-Aldrich Co. and used as received.

Synthesis. The platinum(II) acetylides **1** and **2** were synthesized following the approach described by Sonogashira,[29] see Chart 1. *trans*-$PtCl_2(P(n\text{-}Bu)_3)_2$,[30] **3**,[9] and **4**[19] were prepared as earlier described. Compound **10** has been reported in the literature,[31] but more details of its synthesis are given here.

4-(5-Iodo-thiophen-2-yl)-2-methyl-3-butyn-2-ol (5). 2,5-Diiodothiophene (5 g, 14.9 mmol) was dissolved in a mixture of 40 mL of tetrahydrofuran and 20 mL of triethylamine under

CHART 1: (a) $HOC(CH_3)_2C{\equiv}CH$, $PdCl_2(PPh_3)_2$, PPh_3, CuI, THF/TEA. (b) n-C_5H_{11}−$C_6H_4C{\equiv}CH$, $PdCl_2(PPh_3)_2$, PPh_3, CuI, THF/TEA. (c) NaH, toluene. (d) $PtCl_2(PBu_3)_2$, PBu_3, CuI, THF/DEA. (e) $PtCl_2(PBu_3)_2$, CuI, DEA.

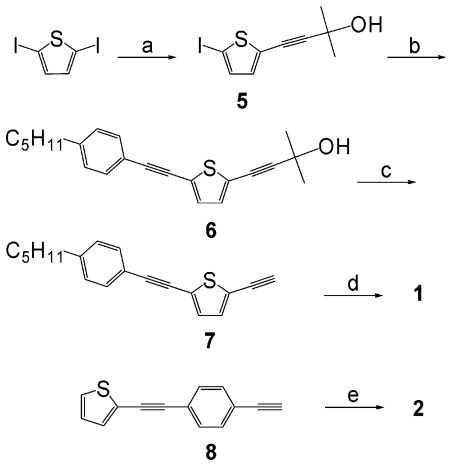

argon. To the solution was added CuI (40 mg, 0.2 mmol), $PdCl_2(PPh_3)_2$ (95 mg, 0.13 mmol), and PPh_3 (0.1 g, 0.4 mmol). The 2-methylbut-3-yn-2-ol (0.84 g, 10 mmol) was added dropwise, and the reaction was allowed to proceed for 48 h at room temperature and at 60 °C for 24 h. The solution was cooled and poured into 100 mL of 1 M HCl. The organic layer was separated, washed with water, and dried, and the solvent was evaporated. Chromatography on silica using a heptane/EtOAc 5:1 mixture as eluent ($R_f = 0.3$) gave the pure product (1.99 g, 68%) as an orange oil. ^{1}H NMR ($CDCl_3$): δ 7.07 (1H, d, J = 4 Hz), 6.8 (1H, d, J = 4 Hz), 2.52 (1H, s), 1.57 (6H, s). ^{13}C NMR ($CDCl_3$): δ 136.8, 133.2, 128.7, 99.3, 74.5, 74.3, 65.6, 31.2.

2-Methyl-4-(5-(4-pentylphenylethynyl)thiophen-2-yl)-3-butyn-2-ol (6). The alcohol **5** (1.0 g, 3.4 mmol) was added to a mixture of 15 mL of THF and 10 mL of triethylamine under argon, followed by CuI (20 mg, 0.1 mmol), $PdCl_2(PPh_3)_2$ (50 mg, 0.07 mmol), and PPh_3 (0.04 g, 0.14 mmol). 4-Pentyl-1-ethynylbenzene (1.0 g, 5.8 mmol) was added dropwise to the solution, which was then heated to reflux for 5 h. The solution was allowed to cool and was poured into 50 mL of 1 M HCl. The organic layer was separated, washed with water, and dried, and the solvent was evaporated. Chromatography of the organic residue on a silica column using heptane/EtOAc 5:1 as eluent ($R_f = 0.4$) yielded 0.98 g (86%) of pure product as a red oil. ^{1}H NMR ($CDCl_3$): δ 7.38 (2H, d, J = 8 Hz), 7.12 (2H, d, J = 8 Hz), 7.05 (1H, d, J = 4 Hz) 7.02 (1H, d, J = 4 Hz), 2.57 (2H, t, J = 8 Hz), 2.44 (1H, s), 1.56 (8H, m), 1.30 (4H, m), 0.88 (3H, t, J = 7 Hz). ^{13}C NMR ($CDCl_3$): δ 143.9, 131.9, 131.4, 128.5, 124.7, 123.6, 119.5, 98.2, 94.1, 81.5, 75.2, 65.7, 35.9, 31.4, 31.2, 30.5, 22.5, 14.0.

2-Ethynyl-5-(4-pentylphenylethynyl)thiophene (7). The alcohol **6** (0.91 g, 2.7 mmol) was dissolved in 100 mL of dry toluene under argon. NaH (0.22 g, 60% dispersion, 5.4 mmol) was added, and 60 mL of the solvent was distilled off. The residue was carefully poured into 50 mL of cold 1 M HCl. The organic phase was removed, evaporated, and filtered through a short silica column. Chromatography of the residue on a silica column using heptane as eluent gave pure product as white crystals, 220 mg (29%). ^{1}H NMR ($CDCl_3$): δ 7.45 (2H, d, J = 8 Hz), 7.17 (3H, dd, J = 8 and 4 Hz), 7.11 (1H, d, J = 4 Hz), 3.38 (1H, s), 2.63 (2H, t, J = 8 Hz), 1.65 (2H, m), 1.35 (4H, m), 0.94 (3H, t, J = 7 Hz). ^{13}C NMR ($CDCl_3$): δ 144.1, 133.0,

131.4, 131.2, 128.5, 125.4, 122.9, 119.5, 94.3, 82.0, 81.3, 76.6. MS (EI, 70 eV): *m*/*z* (%) 221 (91), 278 (M^+, 100), 279 (M + 1, 25).

trans-**Pt(P(*n*-Bu)$_3$)$_2$(C≡C−C$_4$H$_2$S−C≡C-*p*-C$_6$H$_4$-*n*-C$_5$H$_{11}$)$_2$ (1)**. The alkyne 7 (110 mg, 0.395 mmol) was added to a stirred solution of deairated diethyl amine (10 mL) and THF (10 mL), $PtCl_2(P(n\text{-}Bu)_3)_2$ (130 mg, 0.194 mmol), CuI (5 mg, 0.026 mmol), and a few drops of $P(n\text{-}Bu)_3$ at 25 °C under Ar atmosphere. After 3 days the reaction mixture was filtered. The filtrate was diluted with EtOAc and washed three times with 1 M HCl. The organic extract was dried with $MgSO_4$, filtered, and concentrated. Flash chromatography on silica with heptane/ethyl acetate 20:1 gave 200 mg (yield 90%), mp 98 °C. IR: ν(cm^{-1}) = 2088. ^{1}H NMR ($CDCl_3$): δ 7.38 (4H, d, J = 8.0 Hz), 7.12 (4H, d, J = 8.0 Hz), 7.00 (2H, d, J = 3.7 Hz), 6.68 (2H, d, J = 3.7 Hz), 2.58 (4H, t, J = 7.7 Hz), 2.12−2.05 (12H, m), 1.62−1.50 (16H, m), 1.50−1.39 (12H, m), 1.35−1.25 (8H, m), 0.93 (18 H, t, J = 7.2 Hz), 0.87 (6H, t, J = 6.8 Hz). ^{13}C NMR ($CDCl_3$): δ 143.3, 131.5, 131.4, 131.2, 128.4, 127.1, 120.2, 119.7, 116.3 (≡C−Pt(P)$_2$, d,$^1J_{CPt}$ = 985 Hz, t,$^2J_{CP}$ = 14.3 Hz), 101.3, (**C**≡C−Pt, d,$^2J_{CPt}$ = 280 Hz), 92.2, 82.7, 45.7 (imp.), 35.8, 31.4, 30.8, 26.3 (br s), 24.3 (t, J_{CP} = 7.1 Hz), 23.9 (t, J_{CP} = 16.7 Hz), 22.5, 14.0, 13.8, 8.6 (imp.). ^{31}P NMR ($CDCl_3$, relative to ext. H_3PO_4, δ = 0): δ 4.1 (s, d,$^1J_{PtP}$ = 2319 Hz). MS (ESI): *m*/*z* (% relative int. of M^+ peaks) 1153 (41), 1154 (96), 1155 (100), 1156 (76).

trans-**Pt(P(*n*-Bu)$_3$)$_2$(C≡C-*p*-C$_6$H$_4$−C≡C−C$_4$H$_3$S)$_2$ (2).** To a solution of deairated diethyl amine (25 mL), $PtCl_2(P(n\text{-}Bu)_3)_2$ (180 mg, 0.27 mmol), and CuI (8 mg, 0.042 mmol) was added 3 equiv of alkyne **8**[32] (168 mg, 0.84 mmol) at 25 °C under Ar atmosphere. After 3 h, the reaction mixture was worked up and chromatographed on silica gel with toluene/heptane 1:2. An orange powder, 46 mg (yield 16.8%) was obtained, mp 145 °C. TLC R_f = 0.3 (1:2 toluene/heptane). IR: ν(cm^{-1}) = 2094. ^{1}H NMR ($CDCl_3$): δ 7.35 (4 H, d, J = 8.4 Hz), 7.24−7.27 (4 H, m), 7.22 (4 H, d, J = 8.4 Hz), 7.00 (2H, dd, J = 3.7 and 5.1 Hz), 2.09−2.16 (12 H, m), 1.56−1.66 (12 H, m), 1.40−1.49 (12 H, m), 0.92 (18 H, t, J = 7.3 Hz). ^{13}C NMR ($CDCl_3$): δ 131.5, 131.0, 130.6 (br), 129.2 (br), 127.0, 126.9, 123.7, 118.8, 112.1 (≡C−Pt(P)$_2$, d,$^1J_{CPt}$ = 974 Hz, t,$^2J_{CP}$ = 14.5 Hz), 109.3 (C≡C−Pt, d,$^2J_{CPt}$ = 270 Hz), 93.7, 82.9, 26.3, 24.4, (t, J_{CP} = 7 Hz), 23.9 (t, J_{CP} = 17.3 Hz), 13.8. ^{31}P NMR ($CDCl_3$, relative to ext. H_3PO_4, δ = 0): δ 3.8 (s, d,$^1J_{PtP}$ = 2346 Hz). MS (ESI): *m*/*z* (% relative int. of M^+ peaks) 1014 (73), 1015 (100), 1016 (96), 1017 (46).

trans-**Pt(P(*n*-Bu)$_3$)$_2$(C≡C-*p*-C$_6$H$_4$−C≡C-*p*-C$_6$H$_4$−OCH$_3$)$_2$ (9).** *trans*-$PtCl_2(P(n\text{-}Bu)_3)_2$ (309 mg, 0.460 mmol), (4-(4-methoxy-phenylethynyl)-phenyl)-ethyne[33] (214 mg, 0.920 mmol), and a catalytic amount of CuI were dissolved in TEA (6 mL) and THF (6 mL). The reaction flask was placed in a preheated 60 °C oil bath for 5 min. The mixture was allowed to reach room temperature, diluted with $CHCl_3$, and washed three times with 1 M HCl(aq). The organic extract was dried with $MgSO_4$, filtered, and concentrated. Flash chromatography over silica (heptane/EtOAc 20:1, 10:1, 0:1,) gave 446 mg (yield 91%) as light-yellow crystals, mp 177 °C. IR: ν(cm^{-1}) = 2096. ^{1}H NMR ($CDCl_3$): δ 7.45 (4 H, d, J = 8.9 Hz), 7.35 (4 H, d, J = 8.4 Hz), 7.22(4 H, d, J = 8.4 Hz), 6.88 (4 H, d, J = 8.9 Hz), 3.82 (6 H, s), 2.18−2.08 (12 H, m), 1.66−1.55 (12 H, m), 1.50−1.40 (12 H, m), 0.93 (18 H, t, J = 7.3 Hz). ^{13}C NMR ($CDCl_3$): δ 159.4, 132.9, 131.1, 130.6, 128.8, 119.5, 115.7, 113.9, 111.4 (≡C−Pt(P)$_2$, d,$^1J_{CPt}$ = 976 Hz, t,$^2J_{CP}$ = 14.1 Hz), 109.3 (**C**≡C−Pt, d,$^2J_{CPt}$ = 271 Hz), 89.7, 88.7, 55.3, 26.3, 24.4 (t, J_{CP} = 6.5 Hz), 23.9 (t, J_{CP} = 17 Hz), 13.8. ^{31}P NMR ($CDCl_3$, relative to ext. H_3PO_4, δ = 0): δ 3.6 (s, d,$^1J_{PtP}$ = 2350 Hz).

trans-**Pt(P(*n*-Bu)$_3$)$_2$(C≡C-*p*-C$_6$H$_4$−C≡C-*p*-C$_6$H$_4$−NO$_2$)$_2$ (10).**[31] *trans*-$PtCl_2(P(n\text{-}Bu)_3)_2$ (239 mg, 0.356 mmol), (4-(4-nitro-phenylethynyl)-phenyl)-ethyne[34,35] (176 mg, 0.712 mmol), and a catalytic amount of CuI were dissolved in TEA (7 mL) and THF (7 mL). The reaction and the workup were done as described for **9**. Flash chromatography over silica (heptane/EtOAc 14:1) gave 361 mg (yield 93%) as yellow crystals, 168 °C. IR ν(cm^{-1}) = 2208, 2094. ^{1}H NMR ($CDCl_3$): δ 8.21 (4 H, d, J = 8.9 Hz), 7.63 (4 H, d, J = 8.9 Hz), 7.41 (4 H, d, J = 8.4 Hz), 7.26 (4 H, d, J = 8.4 Hz), 2.24−2.04 (12 H, m), 1.70−1.56 (12 H, m), 1.52−1.37 (12 H, m), 0.93 (4 H, t, J = 7.3 Hz). ^{13}C NMR ($CDCl_3$): δ 146.9, 132.2, 131.7, 131.0, 130.7, 130.3, 123.8, 118.1, 113.4 (≡C−Pt(P)$_2$, d,$^1J_{CPt}$ = 980 Hz, t,$^2J_{CP}$ = 15.0 Hz), 109.6 (**C**≡C−Pt, d,$^2J_{CPt}$ = 271 Hz), 95.8, 88.4, 26.5, 24.5 (t, J_{CP} = 7 Hz), 24.1 (t, J_{CP} = 16 Hz), 13.9. ^{31}P NMR ($CDCl_3$, relative to ext. H_3PO_4, δ = 0): δ 3.8 (s, d,$^1J_{PtP}$ = 2340 Hz).

Measurements and Instrumentation. ^{1}H, ^{13}C, and ^{31}P NMR were carried out on a Bruker DRX 400 MHz. ^{1}H and ^{13}C chemical shifts are reported relative to TMS as internal reference, while ^{31}P chemical shifts are given relative to external 0.1 M $P(C_6H_5)_3$ in $CDCl_3$ with δ = −4.89, which corresponds to δ = 0 for 85% H_3PO_4. $CDCl_3$ was used as solvent for the NMR measurements. IR spectra were recorded on neat compounds on a Mattson ATI 60AR FTIR equipped with a Golden Gate Single Reflection Diamond ATR accessory. Mass spectra were obtained from either of two instruments: (1) a JMS-SX/SX102A double focusing magnetic sector mass spectrometer (Jeol, Tokyo), using direct inlet and electron impact ionization (EI+), with ionizing voltage 70 eV, acceleration voltage 10 kV, and resolution 1000; or (2) a Waters Micromass ZQ quadrupole MS using direct inlet, electrospray ionization (ESI), and a sampling cone voltage of 40 V. Optical limiting spectra were recorded with a f/5 focusing system using a frequency-doubled Nd:YAG laser delivering 5-ns pulses at 532−610 nm with a repetition rate of 10 Hz.[36,37] OPL data were obtained for 0.03 M THF solutions in 2-mm quartz cuvets. UV−visible spectra were recorded on a Shimadzu UV-3101PC spectrophotometer in dual mode using 10-mm quartz cells and THF as solvent and repeated on a Shimadzu UV-1601PC spectrometer for the fluorescence quantum yield measurements.

A mode-locked titanium:sapphire laser (Coherent Mira 900-F) was used as excitation source for the luminescence measurements. The pulse repetition frequency was reduced from 76 MHz to the range 4.75 MHz−9.0 kHz using an acousto-optic modulator (Coherent 9200 Pulse Picker). For the steady-state luminescence and time-resolved measurements, the fundamental laser beam (740 nm) was frequency doubled to 370 nm using a SHG crystal (Inrad Ultrafast Harmonic Generation System, Model 5−050). The emission spectra and emission decay traces were taken on a Jobin Yvon IBH FluoroCube spectrometer using the multichannel scaling and the time-correlated single-photon counting modes. IBH DataStation v 2.1 software was used for operation of the spectrometer.

The fluorescence quantum yields were determined relative to the quantum yields of a reference system of Quinine Sulfate (0.546) and Coumarin 110 (0.6).[38] The data were analyzed according to a procedure reported by Williams et al.[39] and "A Guide to Recording Fluorescence Quantum Yields" from Jobin Yvon Inc.[40] Further details on the experimental procedure for photophysical characterization will be published elsewhere.[41]

TABLE 1: Crystallographic Data and Refinement Results of 1 and 2 (ESD Values Are Given in Parentheses)

molecular formula	C62 H88 P2 Pt S2	C52 H68 *P*2 Pt S2
cryst syst	triclinic	triclinic
space group	P-1	P-1
a (Å)	15.0379(4)	10.2292(5)
b (Å)	15.5099(5)	13.4827(6)
c (Å)	20.1090(5)	19.9805(10)
α (deg)	94.723(2)	72.402(3)
β (deg)	107.609(2)	87.443(3)
γ (deg)	93.353(1)	68.678(3)
volume (Å^3)	4438.0(2)	2440.3(2)
cell formula units	3	2
crystal dimensions (mm^3)	0.43 × 0.14 × 0.10	0.34 × 0.14 × 0.12
ρ_{calc} (g•cm^{-3})	1.296	1.380
diffractometer	Bruker-Nonius KappaCCD	Bruker-Nonius KappaCCD
radiation	Mo Kα	Mo Kα
μ (Mo Kα) (mm^{-1})	2.53	3.059
absorption correction	multiscan, SORTAV [45]	multiscan, SORTAV [45]
min/max transmission	0.645/0.776	0.536/0.693
scan type	φ scans and ω with κ offsets	φ scans and ω with κ offsets
$2\theta_{max}$ (deg)	55.76	55.76
temperature (K)	100	100
total data	21173	11277
observed data ($I > 2\sigma(I)$)	15164	9640
method of structure solution	direct methods, SIR 97[43]	direct methods, SIR 97[43]
method of refinement	full least-squares refinement on F^2, SHELXL-97[44]	full least-squares refinement on F^2, SHELXL-97[44]
treatment of hydrogens	riding model	riding model
$R1(F_o > 4\sigma(F_o))/R1$ (all data)	0.0380/0.0641	0.0285/0.0332
$wR2/F_o > 4\sigma(F_o))/wR2$ (all data)	0.0800/0.0888	0.1111/0.1152
no. parameters	907	517
goodness-of-fit (for F^2)	0.80	0.998
residual electron density (max/min)(eÅ^3)	3.525/−1.957	1.614/−2.440
data deposited	Cambridge Structural Database	Cambridge Structural Database

Crystal Structure Determination. Single crystals of **1** and **2** were obtained from heptane at room temperature. The crystal structures were determined from single-crystal X-ray diffraction data at 100 K. Crystals of both **1** and **2** were mounted on the top of glass fibers and data were collected on a Nonius Kappa charge-coupled device (CCD) area detector diffractometer (Mo Kα radiation, graphite monochromator). Data reduction was performed using HKL DENZO and SCALEPACK.[42] The structures were solved by direct methods using SIR97.[43] Fourier calculations and subsequent full-matrix least-squares refinements were carried out using SHELXL97.[44,45] The crystallographic data and detailed structure refinement information are shown in Table 1. All H atoms were positioned geometrically and refined as riding atoms.

Molecular Orbital Calculations. Structure optimizations and frequency calculations were performed with the B3LYP three-parameter hybrid functional[46] and the LANL2DZ effective core potential (ECP) basis set,[47] using GAUSSIAN 03 software.[48] Excitation energies were calculated at the time-dependent (TD) DFT level using the B3LYP functional and the LANL2DZ ECP in GAUSSIAN 98W. Each structure was solved for eight singlet and eight triplet excited states. No empirical corrections were applied to the calculated energies.

Results and Discussion

Structural Considerations. Although the exact nature of the bonding between C and Pt in Pt(II) alkynyl complexes may be difficult to pinpoint, it is often described by σ-type overlap of a C sp hybrid orbital and a Pt hybrid mainly constructed from the 6s, $5d_{x^2-y^2}$, and $5d_{z^2}$ atomic orbitals, where the C−Pt−C and the P−Pt−P bonds lie along the *x* and *y* axes, respectively.[49] Mixing of alkyne π and 5d and 6p orbitals also influences the MO levels. Finally, additional bonding of π-type (π-backbonding) may result from overlap of d_{xy} and d_{xz} orbitals with alkyne π_y* and π_z* orbitals, respectively.[49]

Because of the mixing of Pt d and alkyne π* orbitals, electronic singlet excitation may result in unpaired spin density at Pt. If this takes place, spin−orbit coupling may enhance the rate of ISC from the excited *S* state to a *T* state,[21] which can bring about additional excited-state absorption in the triplet manifold and thus provide more efficient nonlinear absorption.

Hence, we are interested in details that can shed light upon the bonding interaction between Pt and the ethynylaryl units. In the following two sections, structure information is presented from NMR, IR, crystallography, and quantum chemistry calculations. After that, data from UV−visible, OPL, and luminescence (steady state and time-resolved) spectroscopy are presented and discussed.

NMR and IR Spectroscopy. In an NMR study of dialkynyl bisphosphine Ni(II), Pd(II), and Pt(II) complexes, Wrackmeyer has argued that π-backbonding from the metal into the C≡C π* orbitals can be probed by ^{195}Pt and ^{13}C chemical shifts.[50] It was concluded that π-backbonding decreases with the metal ion M in the order Ni > Pd > Pt, in for instance compounds *trans*-M(P(*n*-Bu)$_3$)$_2$(C≡C−C$_6$H$_5$)$_2$, as indicated by δC_1 values of 113.1, 112.3, 108.7 and δC_2 values of 120.1, 111.0, 109.7, respectively.[50] (C_1 is the alkyne carbon closest to Pt, Figure 1.) A lower δ value was accounted for by a smaller paramagnetic nuclear shielding.

Compounds *trans*-Pt(P(*n*-Bu)$_3$)$_2$(C≡C-*p*-C$_6$H$_4$−X)$_2$, with X= H, NO_2, and OCH_3, were also included in the study by Wrackmeyer. δC of the two alkyne carbons were found to decrease with X in the order NO_2 > H > OCH_3.

In the present study, we included NMR data for two additional Pt complexes, **9** and **10** (Figure 2), to be able to make a comparison with data from the study by Wrackmeyer. Selected NMR data is given in Table 2. We were more interested in δ of C_1 than of C_2, because C_1 is directly connected to Pt, and because C_2 is bonded to the 2,5-thiophenylene group in **1**, but to a 1,4-phenylene unit in **2**, **3**, **9**, and **10**.

TABLE 2: ^{13}C NMR Chemical Shifts, $^{13}C-^{195}Pt$ and $^{31}P-^{195}Pt$ Coupling Constants and Infrared Wavenumbers for Compounds 1−3, 9, and 10

compd	δC_1[c,d]	$J(C_1-Pt)$[a]	$J(C_2-Pt)$[a]	$J(P-Pt)$[a]	$\nu(C_1\equiv C_2)$[b]
1	116.3	985	280	2319	2088
2	112.1	974	270	2346	2094
3	111.8[c,d]	975[c]	270[c]	2347[c], 2344[d]	2094[c], 2096[d]
9	111.4	976	271	2350	2096
10	113.4	980	271	2340	2094

[a] In Hz. Estimated uncertainty is ±2 Hz for $J(C_1-Pt)$ and ±0.5 Hz for $J(C_2-Pt)$ and $J(P-Pt)$. [b] In cm^{-1}. Estimated uncertainty is ±1 cm^{-1}. [c] This work. [d] Reference 31.

For all compounds, the C_1 signal appears as a triplet due to $^{13}C-^{31}P$ coupling to two magnetically equivalent ^{31}P nuclei. This is consistent with a trans configuration of the alkynyl groups. Both carbons in the $Pt-C_1\equiv C_2$ fragment also show coupling to ^{195}Pt, (^{195}Pt has $I = {}^1/_2$ and a natural abundance of 33.8%). For **3**, **9**, and **10**, δC_1 decreases with the substituent in the order NO_2 > H > OCH_3 (Table 2), that is, in the same order as for the related compounds in the study by Wrackmeyer. The order **10** > **3** > **9**, together with the fact that the values of δC_1 are rather similar for **3** and **9**, indicates that the π-acceptor property of the substituent has more influence than π-donor or inductive effects on δC_1. In the comparison of all five compounds, δC_1 decreases in the order **1** > **10** > **2** > **3** > **9**. The order **1** > **2** (and **1** > **3**) seems reasonable using a Hammett substituents constant scale such as R^-, which describes the ability for π-electron withdrawal from an electron-rich center. The R^- values are +0.06 and −0.10 for 2-thiophenyl and phenyl,[51] respectively, which means that 2-thiophenyl is the better π-electron acceptor. (Note: 2-Thiophenyl is also a better π-donor than phenyl according to the R^+ scale, and its electron-releasing conjugative effect is stronger than the electron-withdrawing effect.[52]) Further, 2-thiophenyl and phenyl have very similar inductive/field properties according to the F scale of Swain and Lupton.[53] Of course, also the more remote groups (including *n*-pentyl in **1** with a weak π-electron-donating property, $R^- = -0.18$), contribute to the π-accepting ability of the alkyne ligand and need to be taken into account in a comparison between **1** and **2**. In other words, it is difficult to draw conclusions from the differences in δC_1 of **1** and **2** (and **3**, **9**, and **10**) based on Hammet substituent constants when several structural factors vary. Possibly, the different geometry of **1** compared to that of **2** and **3** (see the section on molecular geometry below) can provide an explanation: Given that the P−Pt−P bond axis is close to the plane of the thiophene rings in **1**, but nearly perpendicular to the corresponding plane in **2** and **3**, more efficient back-donation from Pt to the extended π^* orbital of the alkyne ligand should occur in **1** since the d_{xz}-type orbital should not be involved in bonding to P.

It is also intricate to rationalize the δC_1 values in terms of greater π-backbonding in **1** compared to that in **10** only on the basis of Hammet substituent constants. The remote NO_2 substituent ($R^- = +0.62$[51]) undoubtedly makes the $-C_6H_4-CC-C_6H_4-NO_2$ group in **10** a stronger π-electron acceptor than the $-SC_4H_2-CC-C_6H_4-C_5H_{11}$ unit is in **1**. But again, a different orientation of the extended π-system in **1** compared to that in **10** may provide an explanation in terms of a better π-donation from Pt when the d_{xz} electrons are not engaged in bonding to P. However, a refined quantum chemical analysis using accurate geometries of the compounds seems required to obtain more insight into the question of π-backbonding.

In studies of various phosphine Pt complexes, it has been suggested that the s-orbital electron density is of importance for the magnitude of $^{195}Pt-^{31}P$ and $^{195}Pt-^{13}C$ coupling constants.[54−57] An inverse relationship between Pt−P bond length (l_{PtP}) and $^1J_{PtP}$ was found for some cis and trans Pt(II) complexes but for a rather large range of l and J.[56] Correlations between the magnitude of the coupling constants and a qualitative estimate of s-electron density was also considered in the study by Wrackmeyer, but no simple relationships were found.[50] It was concluded that other factors in the theoretical expression by Pople and Santry for spin−spin coupling need to be considered, such as energies for ground-to-excited-state transitions.[58]

In spite of these results, we recorded $^1J_{PtC}$, $^2J_{PtC}$, and $^1J_{PtP}$ for **1**−**3**, **9**, and **10** in an attempt to obtain information about the electronic coupling between Pt and the alkyne ligand. The values of $^1J_{PtC}$ decrease in the order **1** > **10** > **9** ≈ **3** ≈ **2** (Table 2), and a similar trend is found for $^2J_{PtC}$, (the $Pt-C_2$ coupling) with **1** > **9** = **10** ≥ **2** = **3**. Thus, J_{PtC} and δC_1 display essentially the same order of decreasing values for the five compounds. If the s-electron density factors were determining the difference in J_{PtC} in this series, **10** would be expected to have the smallest value of $^1J_{PtC}$ because the NO_2 group has a strong inductive withdrawing effect ($F = +0.65$[51]). But as noted by Yoshida,[57] increased Pt−C π-backbonding might result in a greater value of J_{PtC} in two ways: (1) the shortened $Pt-C_1$ bond length may cause enhanced s-character of the Pt σ hybrid orbital and an increase of its electron density; (2) removal of charge from the Pt d orbitals may result in an increase of the s electron density in the Pt σ hybrid orbital due to an increased effective nuclear charge. In view of these possibilities, the decrease of $^1J_{PtC}$ in the order **1** > **10** > **9** ≈ **3** ≈ **2** may at least partly be explained by a different geometry of **1** than that of the other four compounds and an associated decrease of the π-backbonding. However, it may be noted that the OCH_3 group in **9** normally functions as a π-donor ($R^- = -0.55$[51]) and a σ-acceptor ($F = +0.29$[51]), and one might therefore expect **9** to have the smallest values of $^1J_{PtC}$ and $^2J_{PtC}$.

The magnitude of $^1J_{PtP}$ decreases in the order **9** > **3** ≈ **2** > **10** > **1**, which is almost opposite to that of $^1J_{PtC}$ and $^2J_{PtC}$. This is similar to the findings by Wrackmeyer where $^1J_{PtP}$ of *trans*-$Pt(P(n\text{-}Bu)_3)_2(C\equiv C\text{-}p\text{-}C_6H_4-X)_2$ decreased from $X=OCH_3$ (2395 Hz) to H (2371 Hz) to NO_2 (2326 Hz).[50] Since similar and relatively small values of $^1J_{PtP}$ would be expected for **9** and **10** if the magnitude of the coupling constant was solely an effect of withdrawal of s-electron density in the Pt−P bond due to the substituent, one can conclude that an explanation based on inductive effects does not suffice. Again, other effects and/or bond contributions than the σ-type need to be considered. It has been shown that J_{PtP} varies with the P−Pt−P bond angle for *cis*-Pt(II) phosphines having the same Pt−P bond length,[59] which indicates that molecular geometry and Pt electron back-donation to P can be important for the magnitude of J_{PtP}. Moreover, several studies have shown that Pt−P back-bonding in phosphine Pt complexes involves significant $d-\sigma^*$ interaction.[60,61]

The decrease of $^1J_{PtP}$ in the order **9** > **3** ≈ **2** > **10** > **1** may therefore be rationalized in terms of weaker Pt−P bonding when Pt−C π-backbonding is more pronounced. This appears to be an example of cis influence in complexes of heavier transition metal ions, meaning that strengthening of one bond causes a weakening of another bond in cis position to the former. Cis influence is generally weaker than trans influence but has been observed in NMR studies of Pt complexes.[62,63]

Delocalization of π-electrons is generally regarded as an important factor for optical nonlinearity in organic substances.

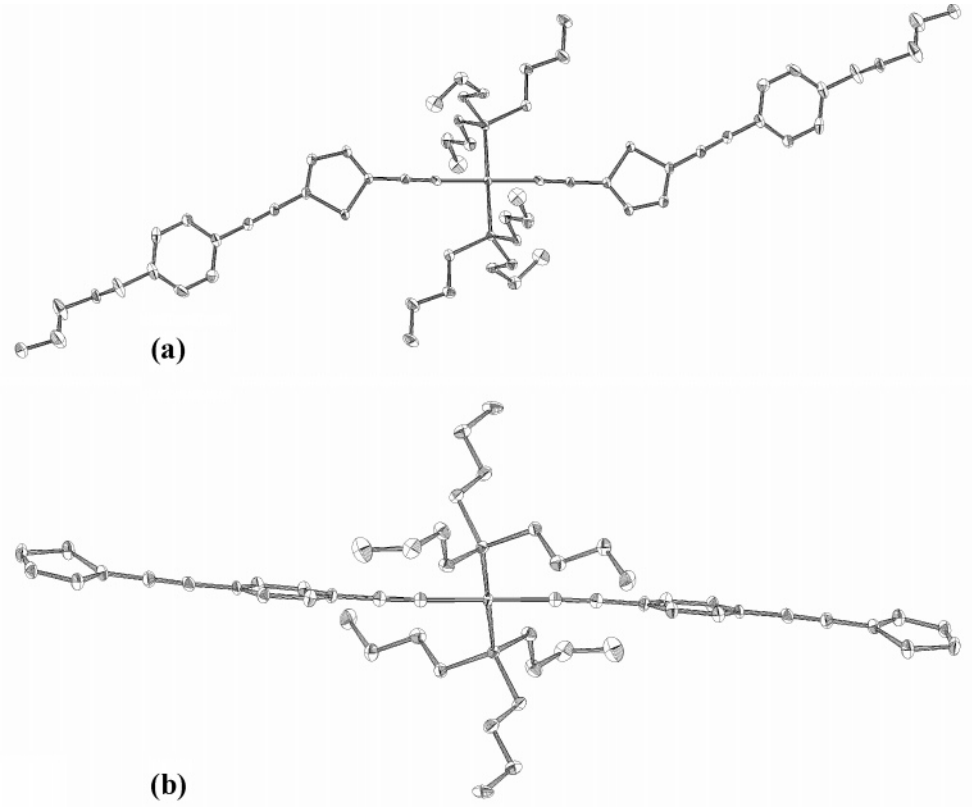

Figure 3. Crystal structure of one of the two symmetry-independent molecules in the unit cell of **1** (a) and **2** (b). Displacement ellipsoids are shown at the 50% probability level.

The infrared stretching frequencies for unsaturated groups in, for instance, dialkynyl bisphosphine Pt complexes can provide information on the degree of delocalization or bond length alternation.[64] We therefore sought information about the Pt−C bond strength in **1**−**3**, **9**, and **10** from C≡C stretching frequencies ($\nu_{C\equiv C}$). A decreased value of ν, related to the $C_1{\equiv}C_2$ bond, was expected to reflect a shortening of the Pt−C_1 bond.[64] The IR spectra of **1**−**3** and **9** showed only one C≡C absorption, in the range of 2088−2096 cm^{-1} (see Table 2). Two C≡C absorptions were found for **10**, at 2094 and 2208 cm^{-1}, and the former was assigned to the Pt−C≡C fragment on the basis of work by Butler.[64] The wavenumbers decrease in the order **3** = **9** > **2** = **10** > **1** and thus imply weaker $C_1{\equiv}C_2$ bonds and reduced bond alternation in that order and that the Pt−C_1 bond strength is greatest for **1**. The value for **2** is more similar to that of **3** than of **1**, as also found for the NMR chemical shifts and coupling constants.

Although data for $\nu_{C\equiv C}$ and J show small differences between the compounds, only slightly greater than experimental uncertainty (Table 2), it is apparent that the IR and NMR data have a consistent trend in that **1** appears to have a stronger Pt− C_1 π-type interaction.

Molecular Geometry from Crystallography and DFT Calculations. The X-ray analyses show that both **1** and **2** have crystal unit cells with two symmetry-independent molecules of similar geometry. All aromatic rings are planar within experimental uncertainty. In **1** (Figure 3a), the aryl rings deviate slightly from coplanarity (maximum of 21°, as measured by angles between least-squares planes), but good conjugation is nevertheless indicated. The Pt−P bonds are aligned along the plane containing the two thiophene rings (the P−Pt−P bond axis is only ca. 1° out of the thiophene planes when sighting along the $C_1{-}C_2$ axis). The four rings are more coplanar in **2** (deviation of max 11°, Figure 3b) than in **1**, and the Pt−P bonds lie ca. 50° out of the plane that contains the inner phenylene rings. Crystallographic data of 3 show that this structure is similar to that of **2**, with only a slight deviation from a common plane for the six-membered rings and with the Pt−P bonds aligned ca. 62° out of that plane.[31] The Pt−C_1 bond lengths in **1**−**3** do not differ significantly (Table 3), which is also true for the $C_1{-}C_2$ bond lengths in **1** and **3**, while those in **2** appears to be slightly longer. The lengths of the Pt−P bonds are slightly shorter in **1** than in **2** and **3**. Hence, these bond lengths do neither support nor oppose the idea from IR $\nu_{C\equiv C}$ and NMR data that there are differences in the Pt−C_1 interaction.

It may also be noted that the C_1−Pt−P bond angles deviate 3−4° from right angles in the X-ray structures for all three compounds. Such deviations appear to be common in crystal structures of Pt(II) acetylides[15] and are also found in the DFT-optimized geometries of the models we employed for **1**−**3** (Table 3 and the following section).

Geometry optimizations of three structures similar to **1**−**3** were performed with the B3LYP functional and the LANL2DZ basis set. To shorten the computational time, the phosphine butyl groups in **1**−**3** and the pentyl groups in **1** were replaced by methyl groups. These three model structures are here denoted **1′**−**3′**. The optimizations were performed starting from three different geometries for **1′** and from two different geometries for each of the other two. When the start structure of **1′** was based on the X-ray structure of **1**, the energy minimum (as established by subsequent frequency calculations) was found to have rather coplanar aromatic rings (a maximum deviation of 15°) and the P−Pt−P axis close to the plane of the rings (9° out of the plane of the thiophene rings).

In the second optimization, the start structure of **1′** had the two phosphine groups relocated so that the P−Pt−P bond axis was close to perpendicular to the plane of the thiophene rings. The geometry optimization resulted in a transition state structure

TABLE 3: Bond Lengths and Bond Angles from Crystallography of Compounds 1−3 and B3LYP/LANL2DZ Calculations of Compounds 1′-3′

	crystallographic bond length (Å)			crystallographic bond angle (deg)			calcd bond length (Å)			calcd bond angle (deg)		
compd	$Pt-C_1$ $Pt-C_{1'}$	C_1-C_2 $C_{1'}-C_{2'}$	$Pt-P_1$ $Pt-P_{1'}$	C_1-Pt-P_1 $C_{1'}-Pt-P_{1'}$	$C_1-Pt-P_{1'}$ $C_{1'}-Pt-P_1$	$P_1-Pt-P_{1'}$	$Pt-C_1$ $Pt-C_{1'}$	C_1-C_2 $C_{1'}-C_{2'}$	$Pt-P_1$ $Pt-P_{1'}$	C_1-Pt-P_1 $C_{1'}-Pt-P_{1'}$	$C_1-Pt-P_{1'}$ $C_{1'}-Pt-P_1$	$C_1-Pt-C_{1'}$	$P_1-Pt-P_{1'}$
1[a] or **1′**[b]	1.997(3)	1.213(4)	2.296(1)	93.2	86.8	180.0	2.008	1.245	2.397	92.2	87.9	180.0	180.0
1[c]	1.996(4)	1.213(5)	2.299(1)	93.9	86.4	179.5	179.4						
	1.994(4)	1.211(5)	2.298(1)	94.1	85.6								
2[d] or **2′**[e]	2.000(3)	1.222(5)	2.306(1)	93.9	86.2	180.0	180.0	2.014	1.242	2.395	92.3	87.7	180.0	180.0
2[d]	1.996(3)	1.220(5)	2.306(1)	93.8	86.2	180.0	180.0							
3[f] or **3′**[e]	1.996	1.214	2.308	93.4	86.6	180.0	180.0	2.014	1.243	2.394	92.3	87.7	180.0	180.0

[a] X-ray at 100 K. Crystals of **1** have two molecules in the unit cell. Row 1 contains data for the molecule with a center of symmetry. [b] Geometry-optimized structure (with Pt−P bonds almost coplanar with the aromatic rings). [c] Rows 2 and 3 contain data for the second molecule in the unit cell, which lacks a center of symmetry. [d] X-ray at 100 K. Crystals of **2** have two molecules in the unit cell, both with a center of symmetry. Data for the two are given in the separate rows. [e] Geometry-optimized structure (with Pt−P bonds almost perpendicular to the plane of the aromatic rings). [f] X-ray at ca. 153 K, ref 31.

Figure 4. Absorption spectra of 10 μM solutions of **1** (circles), **2** (triangles), and **4** (squares) in THF.

with coplanar aromatic rings (maximum deviation of 4°) and a dihedral angle of ca. 77° between the P−Pt−P axis and the plane of the thiophene rings. Notably, this unstable conformation was found to have only 0.2 kcal/mol higher energy that that of the true energy minimum. The third start structure of **1′** was generated by an approximate 180° rotation of one alkyne ligand around the long axis of the molecule, and thus had the S atoms of the thiophene rings on the same side (a syn conformation), instead of on the opposite side as in the X-ray diffraction structure. Again, the optimization found a transition-state structure, with an energy of only 0.05 kcal/mol above that of the true energy minimum.

The optimization of both **2′** and **3′** resulted in only one energy minimum for each structure, irrespective of if the start structures were taken from the X-ray coordinates or were structures having the P−Pt−P axis in the plane of the rings. The optimized structures of **2′** and **3′** have coplanar aromatic rings and ring-plane to Pt−P axis dihedral angles of 89 and 90°, respectively.

The DFT calculations show slightly shorter $Pt-C_1$ and longer C_1-C_2 bonds for **1′**, in comparison with **2′** and **3′** (Table 3), as also indicated by the IR (and NMR) parameters. In contrast to the crystallographic Pt−P bond lengths, which increase slightly from **1** to **2** and **3**, the calculated bond lengths of **1′**−**3′** decrease in the same order. The differences are nevertheless very small.

For all three structures, the DFT-calculated $Pt-C_1$, C_1-C_2, and Pt−P bond lengths are greater than those from crystallography by <1, ca. 3, and ca. 4%, respectively. Thus, the calculated bond lengths are in good to fair agreement with the experimental data. A good agreement is also found for the angles listed in Table 3. Hence, the B3LYP/LANL2DZ model seems to perform well in describing the ground state geometries of Pt(II) arylalkynes such as **1**−**3**, although one should pay attention to the orientation of the Pt−P bonds relative to the plane of the aryl rings and the possibility of more than one coexisting conformation.

The calculations of harmonic vibration frequencies for **1′**−**3′**, undertaken to verify the energy minima, showed only one high-intensity C≡C stretch vibration for each structure. This vibration involves the two inner ethynyl groups (closer to Pt). The unscaled values are 2162, 2174, and 2174 cm^{-1} for **1′**, **2′**, and **3′**, respectively, in fair agreement with the experimental data (Table 2).

UV−Vis Absorption Data and Excitation Energies from TD-DFT Calculations. The absorbance spectra of **1, 2**, and **4** (Figure 4) show that the compounds are quite transparent in

TABLE 4: Absorption Spectral Data of Compounds 1−4 and Excitation Data from TD-B3LYP/LANL2DZ Calculations of Compounds 1′-3′

	exptl		calcd		
compd	λ_{max} (nm)	$\epsilon/10^4$ at λ_{max} (M^{-1} cm^{-1})	λ_{exc} (nm)[a]	f[b]	MOs, coefficients[c]
1 or **1′**	378	8.9	454.1	2.25	H→L, 0.66
			352.0	0.72	H−1→L+1, 0.67
					H→L+2, -0.10
2 or **2′**	362	11	388.6	2.30	H→L, 0.67
			350.8	0.98	H−1→L+1, 0.67
					H→L, 0.12
3 or **3′**	353[d,e]	9.5[d]	368.4	2.49	H→L, 0.67
	350[f]	7.71[e]	330.0	1.09	H−1→L+1, 0.67
	355[g]	8.52 ± 1.80[g]			H→L, 0.13
4	357	10.2			
9	354				
10	395				

[a] Wavelength corresponding to DFT calculated vertical excitation energy for optimized ground state geometry, with oscillator strength above 0.05. [b] Oscillator strength. [c] Molecular orbitals (H = HOMO, L = LUMO) involved in promotion of a single electron, with corresponding wavefunction coefficient above 0.1. [d] In THF, ref 67 and this work. [e] In THF, ref 13. [f] In dichloroethane, refs 9,10. [g] In benzene, ref 14.

the visible region. The absorbance spectra of **3** (not displayed) and **4** are very similar and in accord with those published earlier.[9,13] The spectra of all compounds have similar featureless band shapes, but the absorption maximum of **1** and **10** is red-shifted from that of **4** by ca. 20 and 40 nm, respectively, while **2** and **9** have approximately the same values as **4** (Table 4). Although the value of λ_{max} for **10** is larger than for **1**, instead of the opposite, the order of increasing λ_{max} (**3** ≈ **9** ≈ **4** ≤ **2** < **1** < **10**) indicates that an increase in π-backbonding, as suggested by our NMR and IR data, has some relationship to the red-shift of the absorption band. Because a π*-orbital in a square-planar metal π-ligand complex normally is higher in energy than the metal d orbitals,[65] a d−π* interaction (greater π-backbonding) should result in stabilization of the d orbital and destabilization of the π* orbital. Therefore, the explanation of a relationship between wavelength of absorption and degree of π-backbonding has to include also the occupied π orbital(s) involved in the transition.

In earlier studies of **3**, the main absorption band has been associated with the $S_0 \rightarrow S_1$ transition,[9,10,16] which is in agreement with a theoretical study of other Pt(II) acetylides by Norman.[66] In that study, one-photon excitations were calculated for structures similar to those of **1**−**3**, but the C_5H_{11} groups in **1** were replaced by hydrogens and the PBu_3 ligands in all three compounds were replaced by PH_3 groups.[66] It was found that the geometry-optimized structures had the Pt−P bonds in the common plane of the aromatic rings, which seems to be preferred when the size of the phosphine ligands are sufficiently small, as also pointed out by others.[15] A TD-DFT method using the B3LYP functional and the Stuttgart/Dresden (SDD) ECP was employed by Norman to calculate the excitation wavelengths for the **1′**−**3′** type of structure, which resulted in values of ca. 450, 419, and 403 nm, respectively. Although the excitation wavelengths were longer than our experimental values of λ_{max}, they decreased in the order **1′** > **2′** > **3′**, with a greater difference between **1′** and **2′** (31 nm) than between **2′** and **3′** (15 nm), which is in good agreement with the measured data.

In the present work, TD-B3LYP calculations were performed with the LANL2DZ potential on the geometry-optimized structures. The calculated value for the main excitation of **1′** is 454 nm, in accord with Norman's results, while **2′** and **3′** (with the different orientation of the Pt−P bonds) have the values of 389 and 368 nm, respectively (Table 4). These excitations all have oscillator strengths (f) of 2−2.5. In addition, the calculations revealed a second singlet excitation for **2′** and **3′** at ca. 40−50 nm shorter wavelength, with $f \approx 1$. Structure **1′** also shows such an excitation, but at ca. 100 nm shorter wavelength and with $f \approx 0.7$. The low-energy excitation is dominated by the highest-occupied molecular orbital (HOMO) → lowest-unoccupied molecular orbital (LUMO) transition for all structures, while the second one is described mainly by the HOMO−1 → LUMO+1 transition but with a smaller contribution also from HOMO → LUMO. No other excitations with $f \geq 0.05$ were found. Hence, the featureless absorption bands of **1**−**4** are very likely to originate from the HOMO → LUMO type of excitation. The small absorption at ca. 300−320 nm can then be associated with the second singlet excitation at ca. 330−360 nm found for **2′** and **3′**. It can also be noted that one should not, from the calculations in this work, exclude the possibility that **1**−**4** also can exist in other stable conformations, for instance, with the alternative orientation of the Pt−P bond relative to the ring planes. Even minor populations in such conformations will then contribute to the absorption bands in the 300−400-nm region.

Inspection of the HOMO isodensity surfaces of **2′**, **3′**, and the TS structure of **1′** with the P−Pt−P bond axis nearly perpendicular to the plane of the rings displays a rather uniform π-distribution along the arylalkynyl framework, including the d_{xy} Pt atomic orbital (Figure 5a). The LUMO (also of π-type) has a similar distribution but with a node at Pt. The HOMO of the stable conformation of **1′** is very similar to those of the other structures, but the LUMO surface is somewhat different (Figure 5b). The latter has a significant coefficient at Pt, due to positive mixing of a p orbital at Pt and a π-orbital of the alkyne ligands. A single-point DFT calculation was also performed on **1′** having the X-ray geometry of **1**, where hydrogens were added to the carbons using $C(sp^3)$−H and $C(sp^2)$−H bond lengths of 1.113 and 1.100 Å, respectively. As expected, this calculation revealed virtually identical HOMO/LUMO surfaces as those of the energy minimum of **1′**. The consequence of the LUMO spin density at Pt is that **1** is likely to experience a stronger SOC in the first excited singlet state than for **2**−**4**, since the SOC should manifest itself more effectively when the spin density at the heavy atom is greater.[21] This may cause a faster ISC for **1** compared to that of **2**−**4** (from S_1 to a T state), provided that the S_1-T energy difference is similar for the compounds and that the states have correct symmetry for the transition.[28]

OPL. Previous work on **3** and **4** in THF solution has shown similar OPL properties for these two compounds,[19] and therefore only **4** was utilized for a comparison with **1** and **2**. OPL of 0.030 M solutions of **1**, **2**, and **4** in THF was measured using 5-ns 10-Hz pulses at three wavelengths (532, 550, and 610 nm).

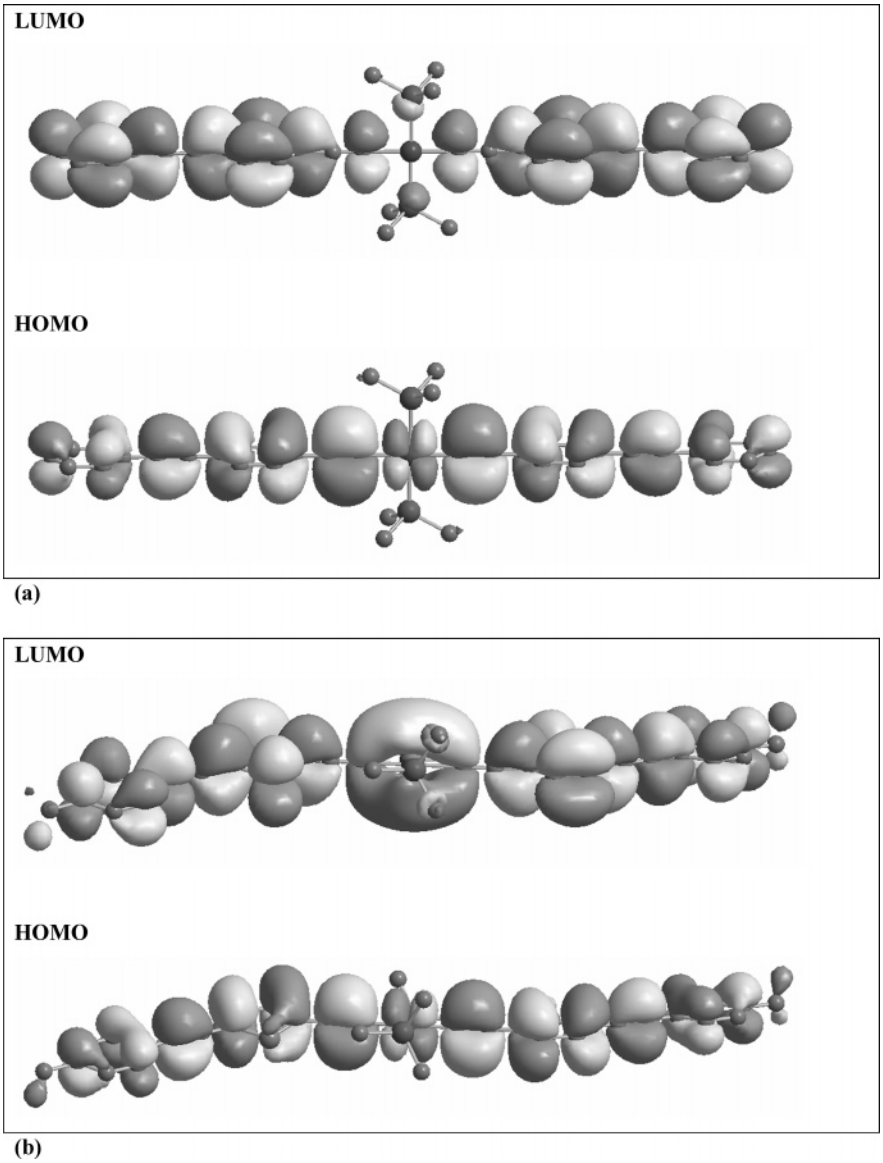

Figure 5. Isodensity HOMO and LUMO surfaces (0.01 a.u.) for B3LYP/LANL2DZ-optimized geometries (slightly tilted and with hydrogens omitted for clarity). (a) Compound **3′** (having the Pt−P bonds out of the plane of the aromatic rings). (b) Compound **1′** (with Pt−P bonds almost coplanar with the aromatic rings).

Plots of transmitted laser energy (E_{out}) vs input energy (E_{in}) show a significant OPL effect for all three compounds at 532 nm (Figure 6a and Table 5). However, the OPL of **2** is somewhat less than that of **1** and **4**; for instance with the values of $E_{out} \approx 7.6\ \mu J$ for **2** compared to $\sim 5\ \mu J$ for **1** and **4** at $E_{in} = 150\ \mu J$. At 550 nm, the OPL of the three compounds is weaker, and that of **1** is intermediate between **2** and **4** (Figure 6b). At 610 nm, the OPL is further diminished but less so for **4** than for **1** and **2**, which have similar values of $E_{out} \approx 25-26\ \mu J$ at $E_{in} = 150\ \mu J$ (Figure 6c). Taken together, we find that the OPL is very dependent on the wavelengths for **1** and **2** in comparison with **4** and that the introduction of the thiophene ring does not improve the optical limiting from that of **4** under these measurement conditions.

Steady State and Time-Resolved Luminescence. The steady-state luminescence spectra of **1**, **2**, and **4** show maximum fluorescence emission at 420, 392, and 390 nm, respectively (Figure 7 and Table 5).[41] Also weak phosphorescence peaks are found at 550 and 526 nm for **2** and **4**, and a very weak peak around 610 nm is observed for **1**.[41]

The Stokes shifts are relatively small (40, 30, and 33 nm for **1**, **2**, and **4**, respectively), which together with the shape of the fluorescence bands are as expected for decay from S_1 states having geometries similar to those of the ground states.

Fluorescence quantum yields were found to be very low, in the range of $0.7-4.5 \times 10^{-3}$.[41] Time-resolved fluorescence was measured with the excitation wavelength of 370 nm for samples with concentrations of approximately 10 μM. The fit of the fluorescence decay of **1**, **2**, and **4** showed a dominant component ($\geq 90\%$) with a decay time of ≤ 2.8 ps, and for **2** and **4** a second component ($\leq 10\%$) with a time constant (τ_{fl}) of a few hundred picoseconds (Table 5). These even shorter fluorescence lifetimes compared to that of 350 ps reported previously for **3** in CH_2Cl_2,[9] together with the low quantum yields, supports the conclusion of a very efficient ISC to a triplet state. An additional explanation for the low quantum yield and fast fluorescence decay has recently been suggested from theoretical work using TD-DFT calculations in our group.[67] A conformation of **3** with PH_3 instead of PBu_3 ligands and with the P−Pt bonds in the plane of the aromatic rings was examined. In addition to the

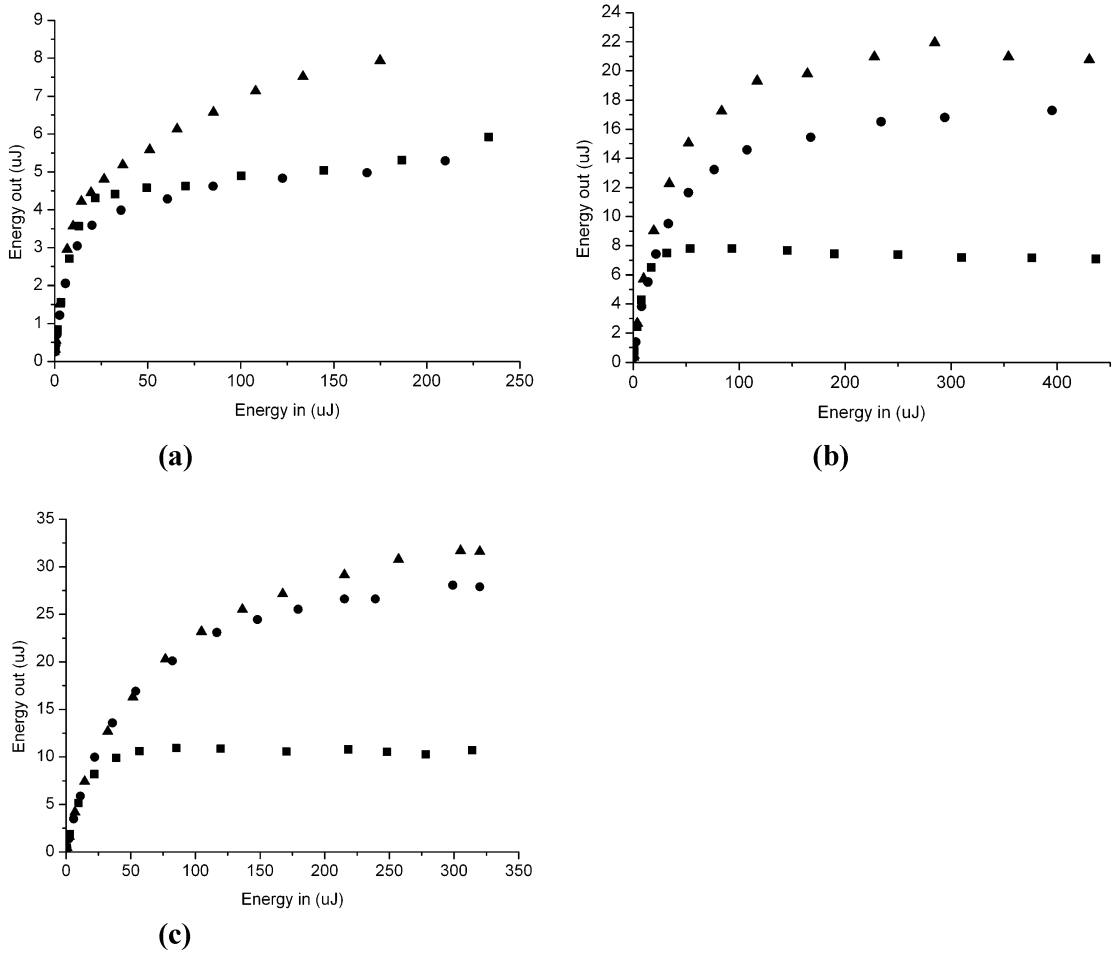

Figure 6. OPL of 0.030 M THF solutions of **1** (circles), **2** (triangles), and **4** (squares) at (a) 532 nm, (b) 550 nm, and (c) 610 nm.

TABLE 5: OPL and Luminescence Spectral Data of Compounds 1−4

	E_{out} (μJ) at $E_{in} = 150$ μJ[a]								
compd	532 nm	550 nm	610 nm	λ_{fl} (nm)[b]	$Q_{fl}/10^{-3}$	Stokes shift (nm)	τ_{fl} (ps)	λ_{phos} (nm)[c]	τ_{phos} (ns)[d]
1	5.0	15	25	420	4.5	40	<2, 94% ~450, 6%	610	190
2	7.6	20	26	392	0.7	30	2.8, 100%	550	330
3				410[e]	2.0		330[e]	520[e]	~500[e]
4	5.2	7.5	11	390	1.1	33	<2, 90% ~350, 10%	525	520

[a] In THF, 30 mM. [b] In THF, $\leq 0.2 \times 10^{-5}$ M. [c] In THF, $0.2-0.3 \times 10^{-4}$ M. [d] Excitation wavelength 380 nm, with 100-kHz pulse repetition frequency. τ_{phos} was measured at λ_{phos} (maximum). Decay times change with concentration and with the amount of oxygen in solution. [e] In dichloroethane at 300 K, ref 9.

dominant $\pi \rightarrow \pi^*$ excitation mentioned above, an excited singlet state at slightly lower energy was found, very weakly coupled to the ground state. By fast internal conversion from the initially populated S_2 state to the dark S_1 state, a pathway using ISC to a T_2 and subsequent T_1 state could be devised on the basis of group theory.[67]

Luminescence spectra were also recorded via two-photon absorption using the mode-locked Coherent Mira 900 set to 740 nm and 1-MHz pulse repetition frequency. The emission spectrum was found to be very similar to the spectrum obtained from single photon excitation (370 nm), which shows that the relaxation proceeds through the same (S_1) state. Weak phosphorescence was found in the region of 500−600 nm, as earlier shown for **3**[9,10] and **4**[19], which is consistent with emission from a triplet state. The phosphorescence decay time was found to decrease in the order **4** > **2** > **1**, with τ values of 520, 330, and 190 ns, respectively. These values are of the same order of magnitude as the decay of approximately 500 ns reported for **3**.[9] The decay rate of the *T* state of **3**[14,17] and **4**[67] is largely determined by quenching due to oxygen in the samples and is likely to be similar for all compounds **1**−**4**. Hence, it is reasonable that the faster decay of the *T* state for **1**, as measured by its phosphorescence, is caused by a more efficient non-radiative $T \rightarrow S_0$ ISC. This can be an effect of contributions to the decay rate from Pt-induced SOC in conformations with significant spin distribution close to the Pt nucleus and from SOC due to the sulfur nucleus and aromatic ring twists.[28]

In light of several studies that have shown support for localization of the long-lived triplet to one of the two arylalkynyl ligands in Pt(II) complexes,[15,17,18,68] it appears necessary to also perform quantum chemical calculations of the relevant triplet states to be able to clarify the path and dynamics of the molecules on the excited-state potential surfaces. Collaborative work along these lines has been initiated in our group.

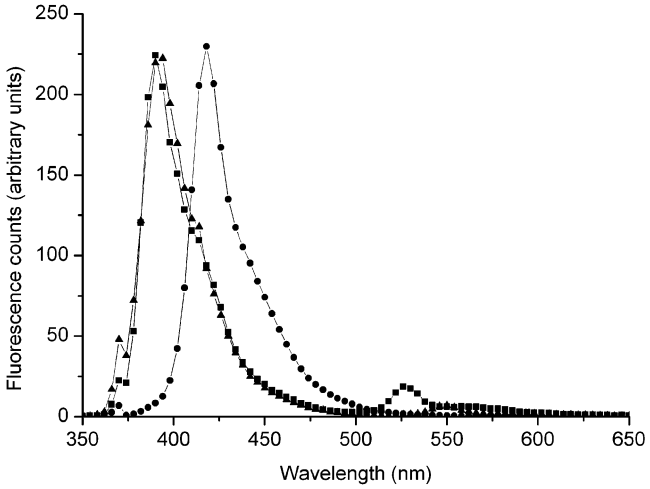

Figure 7. One-photon excited luminescence of **1** (circles), **2** (triangles), and **4** (squares). Excitation wavelength at 370 nm (frequency doubled 740 nm) at 1-MHz pulse repetition frequency.

The similar magnitude of OPL of **1** and **4** at 532 nm could be taken as support for the same mechanisms and rates of the underlying processes of the OPL for the two compounds, most likely involving excited-state absorption from a triplet state. But in view of the significantly shorter *T* lifetime of **1**, additional differences in the dynamics of the $S_0 \rightarrow S_1 \rightarrow T \rightarrow S_0$ channels are probably operative for **1** vs **4**. For instance, a faster depopulation of the triplet manifold for **1** as compared with **4** may be compensated for by an efficient repopulation of the same state during the 5-ns laser pulse at 532 nm. Except for the rates of population and depopulation of the triplet states, the wavelength dependence of the OPL for **1**, **2**, and **4** may have its origin in different absorption profiles of the triplet states. Multiphoton absorption processes, in relation to laser pulse length and intensity, and excitation frequency, is also of importance for the dynamics of the triplet states.[69] Investigations of the TPA cross sections of the compounds in this series will be reported in a separate communication.[41]

Conclusions

Although IR $C_1{\equiv}C_2$ stretch frequencies and NMR δC_1, J_{PtC}, and J_{PtP} values differ only slightly between compounds **1**−**3**, **9**, and **10**, the data support a simple scheme where an increased π-donation from Pt to the alkynyl ligand can be probed by *decreasing* $\nu_{C_1{\equiv}C_2}$ or J_{PtP} or *increasing* δC_1, J_{PtC_1}, or J_{PtC_2}. The NMR and IR data indicate a stronger bonding between C_1 and Pt in **1** compared to **2** and **3**. However, the Pt−C_1, C_1−C_2, and Pt−P bond lengths determined by X-ray crystallography are rather similar for **1**−**3** and do not lend further support for a stronger Pt−C_1 bond in **1**.

The crystallography data show a different conformation of **1** than of **2** and **3**, which also is supported by DFT calculations on models of the three compounds. In the preferred conformation of **1**, the P−Pt bonds are almost coplanar with the aromatic rings. The stable conformations of **2** and **3** have the P−Pt bonds almost at right angles to the planes of the rings. As a result of the different conformations, the spin density at the Pt nucleus is increased in **1** during vertical excitation by near-UV light, while this is not found for **2** and **3**, according to TD-DFT calculations. A larger spin density at Pt in **1** may at least partly account for its comparatively fast fluorescence and phosphorescence decays, via a stronger spin−orbit coupling and a more efficient intersystem crossing. Although the rate of decay from the triplet manifold probably contributes to less efficient OPL for **1** and **2** in comparison with **4** at 550 and 610 nm, several other factors that have not been investigated here remain to be studied in order to delineate the relevant processes for OPL in these compounds.

Acknowledgment. This work was supported (B.E., A.E., M.L.) by a Swedish Defence Nanotechnology Programme run jointly by the Swedish Defence Research Agency (FOI) and Defence Material Administration (FMV). M.L. acknowledges a grant from The Research Council of Norway within the NanoMat program, Contract No. 163529.

Supporting Information Available: Crystallographic information files (in CIF format). This material is available free of charge via the Internet at http://pubs.acs.org.

References and Notes

(1) Zyss, J. *Molecular Nonlinear Optics: Materials, Physics, and Devices*; Academic Press: Boston, 1994.
(2) Stegeman, G. I. Applications of organic materials in third-order nonlinear optics. In *Nonlinear Opt. Org. Mol. Polym.*; Nalwa, H. S., Miyata, S., Eds.; CRC Press: Boca Raton, 1997; p 799.
(3) Teng, C.-C. High-speed electro-optic modulators from nonlinear optical polymers. In *Nonlinear Opt. Org. Mol. Polym.*; Nalwa, H. S., Miyata, S., Eds.; CRC Press: Boca Raton, 1997; pp 441.
(4) Cifuentes, M. P.; Humphrey, M. G. *J. Organomet. Chem.* **2004**, *689*, 3968.
(5) Powell, C. E.; Humphrey, M. G. *Coord. Chem. Rev.* **2004**, *248*, 725.
(6) Vlcek, A., Jr. *Coord. Chem. Rev.* **2000**, *933*, 200−202.
(7) Sun, S.-S.; Lees, A. J. *Coord. Chem. Rev.* **2002**, *230*, 171.
(8) Davey, A. P.; Page, H.; Blau, W.; Byrne, H. J.; Cardin, D. J. *Synth. Met.* **1993**, *57*, 3980.
(9) McKay, T. J.; Bolger, J. A.; Staromlynska, J.; Davy, J. R. *J. Chem. Phys.* **1998**, *108*, 5537.
(10) McKay, T. J.; Staromlynska, J.; Wilson, P.; Davy, J. *J. Appl. Phys.* **1999**, *85*, 1337.
(11) Staromlynska, J.; McKay, T. J.; Wilson, P. *J. Appl. Phys.* **2000**, *88*, 1726.
(12) McKay, T. J.; Staromlynska, J.; Davy, J. R.; Bolger, J. A. *J. Opt. Soc. Am. B: Opt. Phys.* **2001**, *18*, 358.
(13) Cooper, T. M.; McLean, D. G.; Rogers, J. E. *Chem. Phys. Lett.* **2001**, *349*, 31.
(14) Rogers, J. E.; Cooper, T. M.; Fleitz, P. A.; Glass, D. J.; McLean, D. G. *J. Phys. Chem. A* **2002**, *106*, 10108.
(15) Haskins-Glusac, K.; Ghiviriga, I.; Abboud, K. A.; Schanze, K. S. *J. Phys. Chem. B* **2004**, *108*, 4969.
(16) Cooper, T. M.; Blaudeau, J. P.; Hall, B. C.; Rogers, J. E.; McLean, D. G.; Liu, Y. L.; Toscano, J. P. *Chem. Phys. Lett.* **2004**, *400*, 239.
(17) Rogers, J. E.; Hall, B. C.; Hufnagle, D. C.; Slagle, J. E.; Ault, A. P.; McLean, D. G.; Fleitz, P. A.; Cooper, T. M. *J. Chem. Phys.* **2005**, *122*.
(18) Cooper, T. M.; Krein, D. M.; Burke, A. R.; McLean, D. G.; Rogers, J. E.; Slagle, J. E.; Fleitz, P. A. *J. Phys. Chem. A* **2006**, *110*, 4369.
(19) Vestberg, R.; Westlund, R.; Eriksson, A.; Lopes, C.; Carlsson, M.; Eliasson, B.; Glimsdal, E.; Lindgren, M.; Malmstrom, E. *Macromolecules* **2006**, *39*, 2238.
(20) Cheng, L. T.; Tam, W.; Marder, S. R.; Stiegman, A. E.; Rikken, G.; Spangler, C. W. *J. Phys. Chem.* **1991**, *95*, 10643.
(21) Khudyakov, I. V.; Serebrennikov, Y. A.; Turro, N. J. *Chem. Rev.* **1993**, *93*, 537.
(22) He, G. S.; Gvishi, R.; Prasad, P. N.; Reinhardt, B. A. *Opt. Commun.* **1995**, *117*, 133.
(23) Kim, O. K.; Lee, K. S.; Woo, H. Y.; Kim, K. S.; He, G. S.; Swiatkiewicz, J.; Prasad, P. N. *Chem. Mater.* **2000**, *12*, 284.
(24) Paa, W.; Yang, J. P.; Rentsch, S. *Synth. Met.* **2001**, *119*, 525.
(25) Rentsch, S.; Yang, J. P.; Paa, W.; Birckner, E.; Schiedt, J.; Weinkauf, R. *Phys. Chem. Chem. Phys.* **1999**, *1*, 1707.
(26) Becker, R. S.; deMelo, J. S.; Macanita, A. L.; Elisei, F. *J. Phys. Chem.* **1996**, *100*, 18683.
(27) Yang, J. P.; Paa, W.; Rentsch, S. *Synth. Met.* **1999**, *101*, 624.
(28) Beljonne, D.; Shuai, Z.; Pourtois, G.; Bredas, J. L. *J. Phys. Chem. A* **2001**, *105*, 3899.
(29) Sonogashira, K.; Fujikura, Y.; Yatake, T.; Toyoshima, N.; Takahashi, S.; Hagihara, N. *J. Organomet. Chem.* **1978**, *145*, 101.
(30) Kauffman, G. B.; Teter, L. A. *Inorg. Syn.* **1963**, *7*, 245.
(31) Bruce, M. I.; Davy, J.; Hall, B. C.; van Galen, Y. J.; Skelton, B. W.; White, A. H. *Appl. Organomet. Chem.* **2002**, *16*, 559.

(32) Zhan, X.; Yang, M.; Xu, G.; Liu, X.; Ye, P. *Macromol. Rapid Commun.* **2001**, *22*, 358.
(33) Mongin, O.; Gossauer, A. *Tetrahedron* **1997**, *53*, 6835.
(34) Lin, J. T.; Wu, J. J.; Li, C.-S.; Wen, Y. S.; Lin, K.-J. *Organometallics* **1996**, *15*, 5028.
(35) Lavastre, O.; Cabioch, S.; Dixneuf, P. H.; Vohlidal, J. *Tetrahedron* **1997**, *53*, 7595.
(36) Vincent, D. *MCLC S&T, Section B: Nonlinear Optics* **1999**, *21*, 413.
(37) Vincent, D.; Cruickshank, J. *Appl. Opt.* **1997**, *36*, 7794.
(38) Demas, J. N.; Crosby, G. A. *J. Phys. Chem.* **1971**, *75*, 991.
(39) Williams, A. T. R.; Winfield, S. A.; Miller, J. N. *Analyst* **1983**, *108*, 1067.
(40) A Guide to Recording Fluorescence Quantum Yields, http://www.jobinyvon.com/usadivisions/fluorescence/applications/quantumyieldstrad.pdf.
(41) Glimsdal, E.; Carlsson, M.; Eliasson, B.; Minaev, B.; Lindgren, M. *J. Phys. Chem. A* **2007**, *111*, 244.
(42) Otwinowski, Z.; Minor, W. *Methods Enzymol.* **1997**, *276*, 307.
(43) Altomare, A.; Burla, M. C.; Camalli, M.; Cascarano, G. L.; Giacovazzo, C.; Guagliardi, A.; Moliterni, A. G. G.; Polidori, G.; Spagna, R. *J. Appl. Crystallogr.* **1999**, *32*, 115.
(44) Sheldrick, G. M., University of Göttingen, 1997.
(45) Blessing, R. H. *Acta Crystallogr., A* **1995**, *51*, 33.
(46) Becke, A. D. *J. Chem. Phys.* **1993**, *98*, 5648.
(47) Hay, P. J.; Wadt, W. R. *J. Chem. Phys.* **1985**, *82*, 299.
(48) Frisch, M. J.; Trucks, G. W.; Schlegel, H. B.; Scuseria, G. E.; Robb, M. A.; Cheeseman, J. R.; Montgomery, J. A., Jr.; Vreven, T.; Kudin, K. N.; Burant, J. C.; Millam, J. M.; Iyengar, S. S.; Tomasi, J.; Barone, V.; Mennucci, B.; Cossi, M.; Scalmani, G.; Rega, N.; Petersson, G. A.; Nakatsuji, H.; Hada, M.; Ehara, M.; Toyota, K.; Fukuda, R.; Hasegawa, J.; Ishida, M.; Nakajima, T.; Honda, Y.; Kitao, O.; Nakai, H.; Klene, M.; Li, X.; Knox, J. E.; Hratchian, H. P.; Cross, J. B.; Bakken, V.; Adamo, C.; Jaramillo, J.; Gomperts, R.; Stratmann, R. E.; Yazyev, O.; Austin, A. J.; Cammi, R.; Pomelli, C.; Ochterski, J. W.; Ayala, P. Y.; Morokuma, K.; Voth, G. A.; Salvador, P.; Dannenberg, J. J.; Zakrzewski, V. G.; Dapprich, S.; Daniels, A. D.; Strain, M. C.; Farkas, O.; Malick, D. K.; Rabuck, A. D.; Raghavachari, K.; Foresman, J. B.; Ortiz, J. V.; Cui, Q.; Baboul, A. G.; Clifford, S.; Cioslowski, J.; Stefanov, B. B.; Liu, G.; Liashenko, A.; Piskorz, P.; Komaromi, I.; Martin, R. L.; Fox, D. J.; Keith, T.; Al-Laham, M. A.; Peng, C. Y.; Nanayakkara, A.; Challacombe, M.; Gill, P. M. W.; Johnson, B.; Chen, W.; Wong, M. W.; Gonzalez, C.; Pople, J. A. *Gaussian 03*, revision C.02; Gaussian, Inc.: Wallingford, CT, 2004.
(49) Masai, H.; Sonogashira, K.; Hagihara, N. *Bull. Chem. Soc. Jap.* **1971**, *44*, 2226.
(50) Sebald, A.; Wrackmeyer, B.; Beck, W. *Z. Naturforsch., B: Chem. Sci.* **1983**, *38B*, 45.
(51) Hansch, C.; Leo, A.; Taft, R. W. *Chem. Rev.* **1991**, *91*, 165.
(52) Fringuelli, F.; Marino, G.; Taticchi, A. *J. Chem. Soc. B* **1971**, 2302.
(53) Swain, C. G.; Lupton, E. C., Jr. *J. Am. Chem. Soc.* **1968**, *90*, 4328.
(54) Pidcock, A.; Richards, R. E.; Venanzi, L. M. *J. Chem. Soc.* **1966**, 1707.
(55) Allen, F. H.; Pidcock, A. *J. Chem. Soc.* **1968**, 2700.
(56) Mather, G. G.; Pidcock, A.; Rapsey, G. J. N. *J. Chem. Soc., Dalton Trans.* **1973**, 2095.
(57) Miki, S.; Ohno, T.; Iwasaki, H.; Yoshida, Z. I. *J. Phys. Org. Chem.* **1988**, *1*, 333.
(58) Pople, J. A.; Santry, D. P. *Mol. Phys.* **1964**, *8*, 1.
(59) Braterman, P. S.; Cross, R. J.; Manojlovic-Muir, L.; Muir, K. W.; Young, G. B. *J. Organomet. Chem.* **1975**, *84*, C40.
(60) Pacchioni, G.; Bagus, P. S. *Inorg. Chem.* **1992**, *31*, 4391.
(61) Xiao, S. X.; Trogler, W. C.; Ellis, D. E.; Berkovitchyellin, Z. *J. Am. Chem. Soc.* **1983**, *105*, 7033.
(62) Münzenberg, R.; Rademacher, P.; Boese, R. *J. Mol. Struct.* **1998**, *444*, 77.
(63) Appleton, T. G.; Hall, J. R.; Ralph, S. F. *Inorg. Chem.* **1985**, *24*, 4685.
(64) Markwell, R. D.; Butler, I. S.; Kakkar, A. K.; Khan, M. S.; AlZakwani, Z. H.; Lewis, J. *Organometallics* **1996**, *15*, 2331.
(65) Gray, H. B.; Ballhausen, C. J. *J. Am. Chem. Soc.* **1963**, *85*, 260.
(66) Norman, P.; Cronstrand, P.; Ericsson, J. *Chem. Phys.* **2002**, *285*, 207.
(67) Lindgren, M.; Minaev, B.; Glimsdal, E.; Vestberg, R.; Westlund, R.; Malmstrom, E. *J. Lumin.* **2007**, *124*, 302.
(68) Emmert, L. A.; Choi, W.; Marshall, J. A.; Yang, J.; Meyer, L. A.; Brozik, J. A. *J. Phys. Chem. A* **2003**, *107*, 11340.
(69) Baev, A.; Rubio-Pons, O.; Gel'mukhanov, F.; Agren, H. *J. Phys. Chem. A* **2004**, *108*, 7406.